Published in final edited form as:
Neuron. 2006 May 18; 50(4): 589–601. doi:10.1016/j.neuron.2006.04.014.

Differential Compartmentalization and Distinct Functions of $GABA_B$ Receptor Variants

Réjan Vigot[1,10], **Samuel Barbieri**[1,10], **Hans Bräuner-Osborne**[1,2,10], **Rostislav Turecek**[1,3], **Ryuichi Shigemoto**[4,5], **Yan-Ping Zhang**[6], **Rafael Luján**[4,5,7], **Laura H. Jacobson**[8], **Barbara Biermann**[1], **Jean-Marc Fritschy**[9], **Claire-Marie Vacher**[1,11], **Matthias Müller**[8], **Gilles Sansig**[8], **Nicole Guetg**[1], **John F. Cryan**[8,12], **Klemens Kaupmann**[8], **Martin Gassmann**[1], **Thomas G. Oertner**[6], and **Bernhard Bettler**[1,*]

[1]Department of Clinical-Biological Sciences Institute of Physiology Pharmazentrum University of Basel CH-4056 Basel Switzerland [2]Department of Medicinal Chemistry Danish University of Pharmaceutical Sciences DK-2100 Copenhagen Denmark [3]Institute of Experimental Medicine Academy of Sciences 142 20 Prague Czech Republic [4]Division of Cerebral Structure National Institute for Physiological Sciences Myodaiji, Okazaki 444-8585 Japan [5]CREST Japan Science and Technology Corporation Kawaguchi 332-0012 Japan [6]Friedrich Miescher Institute CH-4058 Basel Switzerland [7]Department Ciencias Médicas Facultad de Medicina-CRIB Universidad de Castilla-La Mancha 02006 Albacete Spain [8]Novartis Institutes for BioMedical Research Novartis Pharma AG CH-4002 Basel Switzerland [9]Institute of Pharmacology and Toxicology University of Zurich CH-8057 Zurich Switzerland

Summary

$GABA_B$ receptors are the G protein-coupled receptors for the main inhibitory neurotransmitter in the brain, γ-aminobutyric acid (GABA). Molecular diversity in the $GABA_B$ system arises from the $GABA_{B1a}$ and $GABA_{B1b}$ subunit isoforms that solely differ in their ectodomains by a pair of sushi repeats that is unique to $GABA_{B1a}$. Using a combined genetic, physiological, and morphological approach, we now demonstrate that $GABA_{B1}$ isoforms localize to distinct synaptic sites and convey separate functions in vivo. At hippocampal CA3-to-CA1 synapses, $GABA_{B1a}$ assembles heteroreceptors inhibiting glutamate release, while predominantly $GABA_{B1b}$ mediates postsynaptic inhibition. Electron microscopy reveals a synaptic distribution of $GABA_{B1}$ isoforms that agrees with the observed functional differences. Transfected CA3 neurons selectively express $GABA_{B1a}$ in distal axons, suggesting that the sushi repeats, a conserved protein interaction motif, specify heteroreceptor localization. The constitutive absence of $GABA_{B1a}$ but not $GABA_{B1b}$ results in impaired synaptic plasticity and hippocampus-dependent memory, emphasizing molecular differences in synaptic $GABA_B$ functions.

*Correspondence: bernhard.bettler@unibas.ch.
[10]These authors contributed equally to this work.
[11]Present address: Neurobiologie de l'Olfaction et de la Prise Alimentaire, University of Paris-Sud 11, 91405 Orsay cedex, France.
[12]Present address: Department of Pharmacology and Therapeutics, School of Pharmacy, University College Cork, Cork, Ireland.

Supplemental Data The Supplemental Data for this article are available online at http://www.neuron.org/cgi/content/full/50/4/589/DC1/.

The authors declare no competing financial interest.

Europe PMC Funders Author Manuscripts

Introduction

$GABA_B$ receptors are considered promising drug targets for the treatment of neurological and mental health disorders (Bettler et al., 2004; Cryan and Kaupmann, 2005). Presynaptic $GABA_B$ receptors are subdivided into auto- and heteroreceptors that control the release of GABA and other neurotransmitters, respectively. They restrict neurotransmitter release either by inhibiting voltage-sensitive Ca^{2+} channels or through a direct modulation of synaptic vesicle priming (Mintz and Bean, 1993; Poncer et al., 1997; Sakaba and Neher, 2003). Postsynaptic $GABA_B$ receptors induce slow inhibitory potentials by gating Kir3-type K^+ channels (Lüscher et al., 1997). Considerable evidence has accumulated over the years, using a variety of preparations and techniques, to support the notion that multiple subtypes of $GABA_B$ receptors exist (Bonanno and Raiteri, 1993; Bowery et al., 2002; Cunningham and Enna, 1996; Deisz et al., 1997; Gemignani et al., 1994; Lei and McBain, 2003; Mohler and Fritschy, 1999; Pozza et al., 1999; Yamada et al., 1999). The predicted receptor heterogeneity is not readily supported by molecular studies (Bettler et al., 2004). $GABA_B$ receptors are heterodimers composed of $GABA_{B1}$ and $GABA_{B2}$ subunits, which are both required for normal receptor functioning (Marshall et al., 1999; Mohler and Fritschy, 1999). Accordingly, mice lacking $GABA_{B1}$ (referred to as $1^{-/-}$ mice) or $GABA_{B2}$ subunits show a complete absence of typical $GABA_B$ responses (Gassmann et al., 2004; Prosser et al., 2001; Schuler et al., 2001). The only firmly established molecular diversity in the $GABA_B$ system arises from the $GABA_{B1a}$ and $GABA_{B1b}$ subunit isoforms (Kaupmann et al., 1997). However, no unique pharmacological or functional properties could be assigned to $GABA_{B1a}$ or $GABA_{B1b}$. Most, if not all neurons coexpress $GABA_{B1a}$ and $GABA_{B1b}$, which are generated by differential promoter usage from the *$GABA_{B1}$* gene (Bischoff et al., 1999; Steiger et al., 2004). *$GABA_{B1a}$* and *$GABA_{B1b}$* expression levels vary during development and across individual cells, suggestive of a functional specialization. Structurally, the isoforms differ in their N-terminal ectodomain by a pair of sushi repeats that is present in $GABA_{B1a}$ but not in $GABA_{B1b}$ (Blein et al., 2004). Sushi repeats, also known as complement control protein modules, or short consensus repeats, are found in other G protein-coupled receptors as well (Grace et al., 2004) and mediate protein interactions in a wide variety of adhesion proteins (Lehtinen et al., 2004). The presence of sushi repeats in $GABA_{B1a}$, together with the absence of functional or pharmacological differences in vitro, suggested the existence of auxiliary proteins that modify receptor activity, pharmacology, and localization (Marshall et al., 1999; Mohler and Fritschy, 1999), precedence for which is found with other G protein-coupled receptors (McLatchie et al., 1998). So far, the lack of selective reagents has not allowed addressing the individual contributions of $GABA_{B1a}$ and $GABA_{B1b}$ to native $GABA_B$ functions. In the light of the proposed heterogeneity of native $GABA_B$ receptors, it therefore remains a key question whether $GABA_{B1}$ isoforms exhibit pharmacological and/or functional differences in vivo. Here, we have taken a genetic approach to dissociate the native functions of $GABA_{B1a}$ and $GABA_{B1b}$.

Results

Generation of Mice Selectively Expressing $GABA_{B1a}$ or $GABA_{B1b}$ Subunits

To selectively prevent translation of the $GABA_{B1a}$ and $GABA_{B1b}$ proteins, we converted their initiation codons in the *$GABA_{B1}$* gene into stop codons (Figure 1). Balb/c gene targeting constructs with mutated initiation codons (Figure 1A) were electroporated into Balb/c embryonic stem cells (Dinkel et al., 1999) and homologous recombination events diagnosed with short-arm PCR and Southern blots (data not shown). Targeted embryonic stem cells were injected into C57BL/6 blastocysts. Founder mice were crossed with Balb/c mice expressing Cre-recombinase under control of the cytomegalus virus promoter to excise the neomycin cassette. Pups born from these matings were scored for Cre-mediated loss of the neomycin cassette and bred to homozygosity. Consequently, all mutant mice were on a

pure inbred Balb/c genetic background, which was maintained throughout the experiments. Homozygous mice with mutations in the *GABA$_{B1a}$* (referred to as *1a*$^{-/-}$ mice) or *GABA$_{B1b}$* (*1b*$^{-/-}$ mice) initiation codon were viable, reproduced normally, and exhibited no overt phenotypic abnormalities. Mutant mice showed normal levels of *GABA$_{B1a}$* and *GABA$_{B1b}$* mRNA, indicating that the genetic manipulations do not influence mRNA expression or stability (Figure 1B). Immunoblot analysis revealed the total absence of GABA$_{B1a}$ and GABA$_{B1b}$ protein in *1a*$^{-/-}$ B1b and *1b*$^{-/-}$ mice, respectively, confirming that mutation of the initiation codons prevents translation of the individual subunits (Figure 1C). GABA$_{B1a}$ and GABA$_{B1b}$ proteins appeared upregulated in total brain extracts of knockout mice (Figure 1C), possibly because of increased availability of complementary GABA$_{B2}$ protein, which is required for cross-stabilization (Gassmann et al., 2004). We analyzed whether GABA$_{B}$ protein is also upregulated in the CA1 region of the hippocampus, where the electrophysiological and morphological studies described below were carried out. Similar to those seen in total brain extracts, GABA$_{B1a}$ and GABA$_{B1b}$ protein levels in CA1 extracts were increased in the *1b*$^{-/-}$ (129% of wild-type) and *1a*$^{-/-}$ mice (115% of wild-type), respectively (Figure S1).

Immunohistochemical, Pharmacological, and Biochemical Characterization of *1a*$^{-/-}$ and *1b*$^{-/-}$ Mice

Immunohistochemistry in the CA1 and CA3 region of the hippocampus revealed completely overlapping expression patterns for the GABA$_{B1a}$ and GABA$_{B1b}$ proteins (Figure 2), consistent with an ubiquitous expression of the two proteins in brain neurons (Bischoff et al., 1999). The regional immunostaining in *1a*$^{-/-}$ and wild-type mice was similar, while the staining in *1b*$^{-/-}$ mice was more diffuse and lacked distinct laminar boundaries. Immunohistochemistry therefore suggests differences in the relative abundance of the two isoform proteins at different subcellular sites. For example, intense immunore-activity is evident in CA3 stratum lucidum of *1b*$^{-/-}$ mice, which may hint at a preferential expression of GABA$_{B1a}$ protein at presynaptic sites (arrowhead in Figure 2). The immunostainings obtained with antibodies directed at the GABA$_{B1}$ and GABA$_{B2}$ proteins are similar in the different strains of mice, suggesting that most of the GABA$_{B2}$ and GABA$_{B1}$ protein assembles into heterodimeric receptors. To compare the pharmacology of GABA$_{B1a}$ and GABA$_{B1b}$ in native tissue, we analyzed the inhibition of [^{125}I]CGP64213 antagonist binding (Kaupmann et al., 1997) by GABA and L-baclofen in cortical membranes (Figure 3A). In agreement with recombinant data (Kaupmann et al., 1998), the inhibition curves for wild-type, *1a*$^{-/-}$, and *1b*$^{-/-}$ mice were almost identical (IC$_{50}$ values for wild-type, *1a*$^{-/-}$, and *1b*$^{-/-}$ mice in μM are as follows: GABA: 0.7 ± 0.2, 0.4 ± 0.2, 0.6 ± 0.2; baclofen: 1.2 ± 0.3, 0.8 ± 0.3, 0.9 ± 0.3; n = 3 per genotype). [^{3}H]baclofen binding in *1a*$^{-/-}$ and *1b*$^{-/-}$ cortical membranes was similarly reduced compared to wild-type membranes (Figure 3B), in agreement with the relative abundance of the two isoform proteins in the cortex (Kaupmann et al., 1997). To determine functional GABA$_{B}$ receptor levels, we measured GTPγ[^{35}S] binding, which assesses the activation of Gαi/o-type G proteins, the main effectors of GABA$_{B}$ receptors (Figure 3C). Cortical membranes of *1a*$^{-/-}$ and *1b*$^{-/-}$ mice showed 52% ± 4% and 28% ± 8% of the maximal GTPγ[^{35}S] binding seen with wild-type mice. The sum of the maximal GTPγ[^{35}S] responses in knockout membranes is therefore 20% lower than expected. This suggests the absence of a compensatory upregulation of functional receptor levels, despite the upregulation of GABA$_{B1}$ isoforms seen at the protein level (Figure 1C and Figure S1 in the Supplemental Data available with this article online). Presumably, most of the extra GABA$_{B1}$ isoform protein is retained intracellularly and does not participate in functional responses.

Distinct Contributions of $GABA_{B1a}$ and $GABA_{B1b}$ to Pre- and Postsynaptic $GABA_B$ Functions

Using whole-cell patch-clamp recording in slice preparations, we examined whether wild-type and knockout mice differ in their hippocampal $GABA_B$ responses. We first checked for the presence of heteroreceptors on excitatory terminals. Stimulation of the Schaffer collateral-commissural fibers induces excitatory postsynaptic currents (EPSCs) in CA1 pyramidal neurons, which are reduced by blocking glutamate release through activation of $GABA_B$ heteroreceptors (Schuler et al., 2001). Baclofen, a $GABA_B$ agonist, was effective in reducing the EPSC amplitude in wild-type and $1b^{-/-}$ mice but not in $1a^{-/-}$ mice (Figures 4A and 4B). As a control, adenosine inhibited glutamate release in all three genotypes. This indicates that $1a^{-/-}$ mice, in contrast to $1b^{-/-}$ mice, lack $GABA_B$ heteroreceptors on Schaffer collateral terminals. Small residual heteroreceptor activity in $1a^{-/-}$ mice suggests that minute amounts of $GABA_B$ receptors assembled with $GABA_{B1b}$ are localized at glutamatergic terminals. We next looked for the presence of autoreceptors on GABAergic terminals and recorded inhibitory postsynaptic currents (IPSCs) in the presence of the ionotropic glutamate receptor antagonist kynurenate. Baclofen reduced the amplitude of IPSCs in CA1 pyramidal neurons of all genotypes, suggesting that both $GABA_{B1a}$ and $GABA_{B1b}$ can efficiently participate in autoreceptor function (Figures 4C and 4D). Postsynaptic $GABA_B$ receptors induce a late IPSC by activating Kir3-type K^+ channels (Lüscher et al., 1997). At a holding potential of −50 mV and in physiological extracellular [K^+], baclofen elicited similar outward currents in CA1 pyramidal cells of $1a^{-/-}$ and wild-type mice (Figures 4E and 4F). However, in CA1 pyramidal cells of $1b^{-/-}$ mice, the baclofen-induced outward current was reduced by ~60% compared to wild-type or $1a^{-/-}$ mice. This indicates that predominantly $GABA_{B1b}$ mediates postsynaptic inhibition. As a control, adenosine receptors, which converge on the same Kir3 channels (Lüscher et al., 1997), induced similar outward currents in all genotypes. It is formally possible that the upregulation of $GABA_{B1a}$ protein observed in the $1b^{-/-}$ mice (Figure 1C and Figure S1) compensates to some extent for the missing $GABA_{B1b}$ protein. We consider this unlikely because functional receptor levels in the $1b^{-/-}$ mice are lower than expected (Figure 3C). Moreover, GFP-tagged $GABA_{B1a}$ protein clearly distributes to the dendritic compartment of CA1 neurons when expressed in organotypic slice culture (Figure 6A). Likely, therefore, both $GABA_{B1a}$- and $GABA_{B1b}$-containing receptors address Kir3 channels under normal conditions.

Distinct Subcellular Compartmentalization of the $GABA_{B1a}$ and $GABA_{B1b}$ Proteins

The lack of suitable antibodies thus far prevented studying the distribution of $GABA_{B1}$ isoforms using electron microscopy. We now used the $1a^{-/-}$ and $1b^{-/-}$ mice to determine the subcellular localization of $GABA_{B1b}$ and $GABA_{B1a}$ protein, respectively. Preembedding immunogold labeling experiments in the CA1 stratum radiatum of wild-type mice confirmed that $GABA_{B1}$ protein is present in pre- and postsynaptic elements (Figure 5A), as reported for rat brain (Kulik et al., 2003). In $1a^{-/-}$ mice, $GABA_{B1b}$ was mostly found in spines opposite glutamate release sites (Figures 5B and 5C). In $1b^{-/-}$ mice, $GABA_{B1a}$ predominantly localized to glutamatergic terminals (Figures 5D and 5E). Quantitative analysis of $GABA_{B1}$ labeling showed that the ratio of pre- to postsynaptic immunoparticles in wild-type, $1a^{-/-}$, and $1b^{-/-}$ mice was 0.31, 0.17, and 1.61, respectively (Figure 5F). Thus, the electron microscopy data support the electrophysiological data (Figure 4) and confirm that $GABA_{B1a}$ preferentially localizes to glutamatergic terminals. Consistent with residual heteroreceptor activity (Figures 4A and 4B), some presynaptic immunogold labeling persisted at glutamatergic $1a^{-/-}$ synapses.

Selective Localization of $GABA_{B1a}$ to Axons and $GABA_{B1b}$ to Dendritic Spines in Transfected Hippocampal Neurons

We analyzed whether GFP-tagged $GABA_{B1a}$ and $GABA_{B1b}$ proteins exhibit a distinct subcellular distribution when expressed in hippocampal neurons. For these experiments, we transfected organotypic hippocampal slice cultures, which preserve the basic CA3-CA1 connectivity, with expression vectors coding for $GABA_{B1a}$-GFP or $GABA_{B1b}$-GFP. We coexpressed a freely diffusible red fluorescent protein (RFP), tdimer2, to normalize the green fluorescence to the red fluorescence. Both $GABA_{B1a}$-GFP and $GABA_{B1b}$-GFP proteins were robustly expressed in the dendrites of transfected CA1 pyramidal neurons (Figures 6A, 6B, and 6D). $GABA_{B1b}$-GFP was expressed in the majority of dendritic spines, while $GABA_{B1a}$-GFP was largely excluded from this location. This agrees with the electron microscopy data showing a preferential association of the $GABA_{B1b}$ protein with spines opposite to glutamate release sites (Figures 5B and 5C), a location where Kir3 channels are highly coclustered with $GABA_B$ receptors (Kulik et al., 2006). This may explain why predominantly $GABA_{B1b}$ mediates the activation of Kir3 currents (Figures 4E and 4F). The data further indicate an almost exclusive association of the $GABA_{B1a}$-GFP protein with distal axons (Figure 6), again in agreement with the electrophysiological (Figures 4A and 4B) and morphological data (Figures 5D and 5E).

Impaired Synaptic Plasticity in $1a^{-/-}$ Mice

Activation of postsynaptic $GABA_B$ receptors was shown to restrict long-term potentiation (LTP), whereas activation of autoreceptors promotes LTP (Davies and Collingridge, 1996; Davies et al., 1991). A role for $GABA_B$ heteroreceptors in synaptic plasticity is not known. We therefore addressed whether the genetic loss of heteroreceptors in $1a^{-/-}$ mice affects LTP at CA3-to-CA1 synapses. In wild-type CA1 neurons, the pairing protocol induced a marked potentiation of the EPSC amplitude (268.9% ± 58.3%; n = 7) (Figures 7A and 7B). No LTP developed when NMDA receptors were antagonized (CPP + 7-Cl-kynurenic acid) or when the cell under recording was kept at −70 mV (Figure 7B). $1^{-/-}$ mice, which completely lack functional $GABA_B$ receptors (Schuler et al., 2001), did not exhibit notable LTP (9.4% ± 20.3%; n = 5), nor did $1a^{-/-}$ mice (−8.9% ± 9.3%; n = 9) (Figures 7A and 7B). In contrast, $1b^{-/-}$ mice exhibited normal LTP (228.7% ± 43.3%; n = 5). Wild-type neurons developed LTP even after acute pharmacological blockade of $GABA_B$ receptors with the antagonist CGP54626 (182.8% ± 54%; n = 6), showing that acute blockade of $GABA_B$ receptors does not prevent the induction of LTP. Adaptive changes (see below) due to the constitutive absence of heteroreceptors are therefore expected to underlie the lack of LTP in $1a^{-/-}$ neurons (Figure 7B).

Synaptic Modifications in $1a^{-/-}$ Mice

The amplitude ratio of evoked EPSCs in response to paired-pulse stimulation was similar in wild-type, $1a^{-/-}$, and $1b^{-/-}$ CA1 pyramidal neurons (Figure 7C). A change in the paired-pulse ratio is generally believed to reflect an underlying change in the presynaptic probability of release. The absence of differences in the paired-pulse ratio between the three genotypes therefore provides no evidence for a change in the release probability in $1a^{-/-}$ mice. Moreover, these results indicate that the paired-pulse protocol does not result in the activation of $GABA_B$ heteroreceptors in wild-type neurons, nor do heteroreceptors appear to be tonically activated by ambient GABA, in agreement with earlier studies (Morrisett et al., 1991; Scanziani, 2000). CGP54626 had no effect on the miniature EPSC (mEPSC) frequency or amplitude in wild-type CA1 neurons, further supporting that ambient GABA does not tonically activate heteroreceptors under baseline conditions (Figure 7D). The frequency of spontaneous mEPSCs was significantly increased in $1a^{-/-}$ mice, while the mEPSC amplitude remained similar as in wild-type or $1b^{-/-}$ mice (Figure 7E). The observed increase in the baseline mEPSC frequency in $1a^{-/-}$ mice would normally argue for an

increase in the probability of glutamate release. However, since CA3-to-CA1 synapses in *1a*$^{-/-}$ mice exhibit no change in the pairedpulse ratio and heteroreceptors remain inactive under baseline conditions, we favor that the increase in mEPSC frequency is indicative of an increased number of functional synapses. An increase in mEPSC frequency, with a concomitant modest increase in mEPSC amplitude, has been observed in cultured hippocampal neurons as a consequence of the unmasking of "silent" synapses (Liao et al., 1999). The insertion of AMPA receptors into synapses that only contain NMDA receptors is expected to result in a decrease in the coefficient of variation (CV) of the AMPA receptor-mediated component of the EPSC (CV_{AMPA}), with no change in the CV of the NMDA component (CV_{NMDA}) (Kullmann, 1994). We measured the variability of the AMPA and NMDA receptor-mediated EPSC amplitudes recorded in the same cells at −70 mV and +30 mV, respectively (Figure 7F). We found that the CV_{AMPA} was significantly higher for the wild-type (0.37 ± 0.04; n = 12) than for the *1a*$^{-/-}$ mice (0.24 ± 0.03; n = 10; $p < 0.02$), while the CV_{NMDA} for wild-type (0.23 ± 0.02; n = 12) and *1a*$^{-/-}$ mice (0.22 ± 0.03; n = 10) was similar. Comparison of the CV_{AMPA} and CV_{NMDA} between *1a*$^{-/-}$ and wild-type mice is therefore consistent with a decreased proportion of silent synapses in *1a*$^{-/-}$ mice (Figure 7G).

Impaired Object Recognition in *1a*$^{-/-}$ Mice

Changes in hippocampal LTP accompany certain alterations in cognitive function (Barnes et al., 1994). We used an object recognition task that depends on hippocampal function (Broadbent et al., 2004) to analyze whether impaired presynaptic heteroreceptor inhibition and lack of LTP in *1a*$^{-/-}$ mice is paralleled by memory deficits. The task relies upon the tendency of rodents to attend to a novel object more than to a familiar one. For each mouse, we scored the number of stretch attend postures (SAP, defined as head and shoulders extended toward the object) in response to a PVC disc presented at times 10 min and 24 hr following initial presentation at time 0, as well as to a novel PVC cone at 24 hr + 10 min. Wild-type and *1b*$^{-/-}$ mice, in contrast to *1a*$^{-/-}$ mice, showed a significantly reduced number of SAPs toward the familiar object (time 10 min) and subsequently an increased number of SAPs toward the novel versus familiar object (time 24 hr + 10 min) (Figure 8A). Calculation of discrimination indices (DIs) showed that *1a*$^{-/-}$ mice did not discriminate between familiar or novel objects (Figure 8B). Therefore, in *1a*$^{-/-}$ mice, the lack of LTP is correlated with an impairment of nonspatial hippocampal memory formation. The effects on synaptic plasticity and memory formation in *1a*$^{-/-}$ mice emphasize that the $GABA_{B1b}$ protein cannot compensate for the loss of $GABA_{B1a}$ protein.

Discussion

The objective of this study was to determine if $GABA_{B1a}$ and $GABA_{B1b}$ exhibit functional or pharmacological differences in vivo. Our experiments with genetically modified mice indicate that, at CA3-to-CA1 synapses, $GABA_{B1a}$ assembles heteroreceptors inhibiting glutamate release, while predominantly $GABA_{B1b}$ mediates postsynaptic inhibition (Figure 4). This functional specialization relates, at least in part, to a distinct subcellular distribution of the $GABA_{B1}$ isoforms (Figure 5). Autoreceptor function is unaltered in the *1a*$^{-/-}$ and *1b*$^{-/-}$ mice (Figures 4C and 4D). Possibly, both $GABA_{B1a}$ and $GABA_{B1b}$ are present at GABAergic terminals impinging onto CA1 pyramidal neurons. However, since our recordings from the CA1 pyramidal soma cannot distinguish IPSCs from different types of GABAergic neurons, it is equally possible that some GABAergic terminals express $GABA_{B1a}$ and others express $GABA_{B1b}$. In general, the extent of subcellular segregation of $GABA_{B1a}$ and $GABA_{B1b}$ may vary according to brain regions and cell types. For example, GABAergic neurons impinging onto cortical layer 5 pyramidal neurons express $GABA_{B1a}$ but not $GABA_{B1b}$ at their terminals (Pérez-Garci et al., 2006). The distribution of $GABA_{B1a}$

and $GABA_{B1b}$ may also vary within the dendritic compartment. This is suggested by the organotypic slice culture experiments showing that $GABA_{B1a}$-GFP is mostly excluded from dendritic spines, while $GABA_{B1b}$-GFP is expressed in most spines (Figure 6).

No significant pharmacological differences were found in radioligand binding experiments with cortical membranes from *1b*$^{-/-}$ and *1a*$^{-/-}$ mice (Figure 3). This confirms that $GABA_B$ isoforms display a similar binding pharmacology in vivo, as already suggested by earlier experiments with the photoaffinity antagonist [^{125}I]CGP71872 (Malitschek et al., 1998). Of note, receptors assembled from $GABA_{B1a}$ or $GABA_{B1b}$ may still display pharmacological differences in functional assays, depending on the local effector system and/or the receptor reserve. This may also be the reason why the data obtained in a functional assay (GTPγ[^{35}S] binding) and in ^{3}[H]baclofen binding show differences in the relative contribution to the total binding (Figures 3B and 3C). Depending on the subcellular localization, $GABA_{B1a}$ and $GABA_{B1b}$ may also be exposed to different concentrations of ambient GABA. Tonic activation of $GABA_B$ auto- but not heteroreceptors could, for example, account for different potencies of baclofen in inhibiting release at excitatory and inhibitory terminals (Lei and McBain, 2003; Scanziani, 2000). Moreover, $GABA_{B1a}$ and $GABA_{B1b}$ may exhibit distinct desensitization properties depending on their localization and exposure to cyclic AMP-dependent protein kinase (Couve et al., 2002). These factors may have contributed to pharmacological differences between pre- and postsynaptic receptors reported in the past (Lei and McBain, 2003; Pozza et al., 1999). However, they likely do not explain differences in the rank order of drug potencies at native $GABA_B$ receptors, which have been reported as well (Bonanno et al., 1997; Cunningham and Enna, 1996).

An interesting question is how the functional segregation between the $GABA_{B1a}$ and $GABA_{B1b}$ isoforms is achieved. In principle, receptor compartmentalization could involve mechanisms such as mRNA trafficking, protein targeting, or protein retention (Horton and Ehlers, 2003; Sampo et al., 2003). We addressed the mechanism underlying the differential compartmentalization by expressing GFP-tagged $GABA_{B1a}$ or $GABA_{B1b}$ proteins in hippocampal neurons in organotypic slice cultures. The data show an almost exclusive association of the $GABA_{B1a}$-GFP protein with the axons of transfected CA3 neurons (Figure 6). We therefore favor protein targeting or retention as the reason for $GABA_{B1a}$ compartmentalization, in which case the information for segregation is probably carried by the extracellular pair of sushi repeats, the only region of sequence divergence between $GABA_{B1a}$ and $GABA_{B1b}$. Interestingly, the two sushi repeats in $GABA_{B1a}$ have strikingly different structural properties (Blein et al., 2004). This led to the proposal that they participate in protein interactions with multiple partners, which could generate additional heterogeneity in the $GABA_B$ receptor system.

An open question remains why LTP at CA3-to-CA1 synapses is impaired in *1a*$^{-/-}$ mice. Since autoreceptor and postsynaptic $GABA_B$ functions are preserved in *1a*$^{-/-}$ mice (Figure 4), the impairment of LTP must relate to the constitutive absence of heteroreceptors. Heteroreceptors do not appear to be activated by ambient or released GABA under baseline conditions (Figures 7C and 7D), as already suggested in earlier experiments (Morrisett et al., 1991; Scanziani, 2000). Presumably, heteroreceptors are only activated during periods of intense neuronal activity, when GABA released from interneurons spills over to the glutamatergic terminals. Uncontrolled release of glutamate during such periods is likely to trigger adaptive changes (Burrone and Murthy, 2003). For example, excess released glutamate may spill over to synapses at which glutamate release has not occurred (Scimemi et al., 2004), which could convert silent synapses to a functional state (Isaac et al., 1995; Liao et al., 1995). The observed increase in the mEPSC frequency in *1a*$^{-/-}$ mice (Figure 7E) could reflect such an increase in the rate of activation of previously silent synapses (Liao et al., 1999). We addressed this possibility and compared the CVs of AMPA and NMDA

receptor-mediated EPSCs in wild-type and $1a^{-/-}$ mice. The CV_{AMPA} was significantly reduced in $1a^{-/-}$ mice, while the CV_{NMDA} was unaffected by genotype, consistent with a decreased number of silent synapses in $1a^{-/-}$ mice (Kullmann, 1994). Since silent synapses provide an ideal substrate for LTP (Durand et al., 1996; Isaac et al., 1995; Kullmann, 1994; Liao et al., 1995; Malinow and Malenka, 2002), the observed impairment of LTP in $1a^{-/-}$ mice could be explained by the decrease in the proportion of silent synapses. A plausible physiological role for heteroreceptors could therefore be to limit the loss of silent synapses and to ensure that plasticity processes are maintained in the dynamic range. However, the constitutive absence of heteroreceptors in $1a^{-/-}$ mice may have allowed time for other compensatory adaptations. For example, disinhibition of adenylate cyclase activity (Pineda et al., 2004), transcriptional (West et al., 2002) and/or morphological changes (Luthi et al., 2001) may contribute to the impairment of LTP and hippocampus-dependent memory. Importantly, however, the LTP and behavioral data reinforce that $GABA_{B1a}$ and $GABA_{B1b}$ convey separate functions in vivo.

In summary, our combined physiological, morphological, and behavioral analysis of $1a^{-/-}$ and $1b^{-/-}$ mice clearly establishes that $GABA_{B1a}$ and $GABA_{B1b}$ are differentially compartmentalized and fulfill distinct functions. We hypothesize that interactions with the sushi repeats are responsible for retaining $GABA_{B1a}$ at its specific location. From a pharmaceutical perspective, the existence of functionally distinct receptor subtypes opens up new opportunities for therapeutic interference.

Experimental Procedures

Generation and Pharmacological and Biochemical Characterization of $1a^{-/-}$ and $1b^{-/-}$ Mice

Knockin mice were generated as outlined in Figure 1. All animal experiments were subjected to institutional review and conducted in accordance with Swiss guidelines and approved by the veterinary Office of Basel-Stadt. [^{125}I]CGP64213 was synthesized at Novartis and labeled to a specific radioactivity of >2000 Ci/mmol (ANAWA, Wangen, Switzerland). The probes used for Northern blot analysis, the [^{125}I]CGP64213 displacement experiments, immunoblot, and GTPγ[^{35}S] analysis were as described (Bischoff et al., 1999; Gassmann et al., 2004; Kaupmann et al., 1997). Since we did not observe significant differences in any of our assays between wild-type littermates derived from $1a^{+/-}$ or $1b^{+/-}$ heterozygous breeding pairs, the data from wild-type mice were pooled.

Electrophysiology

Standard procedures were used to prepare 300 μm thick parasagittal hippocampal slices from P18–P28 mice. Slices were incubated for 45 min at 35°C in an interface chamber containing saline (124 mM NaCl, 2.7 mM KCl, 1.3 mM $MgCl_2$, 2 mM $CaCl_2$, 1.24 mM NaH_2PO_4, 26 mM $NaHCO_3$, 18 mM glucose, 2.25 mM ascorbate) equilibrated with 95% O_2/5% CO_2. Slices were then kept at room temperature for at least 45 min before starting recordings at 30°C–32°C. Whole-cell patchclamp recordings were performed from the somata of CA1 pyramidal neurons to measure holding currents and synaptic responses; neurons were visualized using infrared and differential interference contrast optics. Drugs, applied by superfusion into the recording chamber, were kept as aliquots, and solutions were freshly prepared on the day of the experiment. K^+ currents induced by baclofen (50 μM) or adenosine (100 μM) were elicited at −50 mV in the presence of TTX (1 μM). Patch electrodes (~5 MΩ) were filled with a solution containing the following: 140 mM K-gluconate, 5 mM HEPES, 2 mM $MgCl_2$, 1.1 mM EGTA, 2 mM Na_2ATP, 5 mM phosphocreatine, 0.6 mM Tris-GTP, at pH 7.25 with KOH and 285 mOsm). EPSCs and IPSCs were elicited by voltage pulses (100 μs, 2–5 V stimuli) or by current pulses (100 μs,

0.1–0.3 mA stimuli) delivered through a bipolar Pt-Ir electrode (25 μm in diameter) placed in the stratum radiatum at a distance of 150–200 μm from the soma of the recorded cell. The recording electrode was filled with a solution containing the following: 140 mM Cs-gluconate, 10 mM HEPES, 10 mM phosphocreatine, 5 mM QX-314, 4 mM Mg-ATP, 0.3 mM Na-GTP, at pH 7.25 with CsOH and 285 mOsm. EPSCs were measured at −70 mV in the presence of 100 μM picrotoxin. In some cells, stimuli were delivered in pairs (interpulse interval 70 ms) (Palmer et al., 2004), and the paired-pulse ratio (PPR) was calculated as the ratio of the 2nd EPSC amplitude/1st EPSC amplitude. IPSCs were measured at 0 mV in the presence of 2 mM kynurenic acid. For the LTP experiments, the baseline stimulus frequency was set to 0.05 Hz to minimize “rundown” of the EPSC amplitudes (Gasparini et al., 2000; Xiao et al., 2004). Cells were voltage clamped at −70 mV during baseline and recovery periods. LTP was induced by depolarizing the cell to 0 mV while delivering 40 stimuli at 0.5 Hz at baseline stimulus intensity (pairing paradigm) (Palmer et al., 2004). When the potentiation of EPSC amplitudes lasted for >30 min, we considered this as LTP. mEPSCs were recorded at −70 mV in the presence of 0.5 μM TTX and 10 μM bicuculline. Detection and analysis of mEPSCs were done using the MiniAnalysis software (Synaptosoft, Decatur, GA). For analysis of the CV_{AMPA} (Kullmann, 1994), AMPA receptor-mediated EPSCs were recorded in the presence of 100 μM picrotoxin and 5 μM bicuculline while neurons were clamped at −70 mV (0.05 Hz stimulation). Following 15–20 min recording, non-NMDA glutamate receptors were blocked with 10 μM DNQX, and the holding voltage was changed to +30 mV. For analysis of the CV_{NMDA}, NMDA receptor-mediated EPSCs were recorded for >10 min and, as a control, eventually blocked by adding CPP (5 μM) and 7-chlorokynurenate (10 μM) to the superfusion. CV_{AMPA} and CV_{NMDA} were calculated as SD/mean of AMPA and NMDA receptor-mediated EPSC peak amplitudes, respectively. Data were obtained with an Axopatch 200B (Axon Instruments, Union City, CA), filtered at 2 kHz and digitized at 10 kHz, and acquired and analyzed with pClamp9 (Axon Instruments, Union City, CA). Values are expressed as mean ± SEM. The experimenter was blind to the genotype of the mice.

Immunohistochemistry and Preembedding Electron Microscopy

Hippocampal sections were treated for light and electron microscopy immunolabeling as described (Gassmann et al., 2004; Kulik et al., 2002). For ultrastructural analysis, only immunogold particles inside the plasma membrane (closer than 30 nm) of morphologically identifiable terminals (with presynaptic active zone or clear vesicles) and dendrites/spines were counted. Unassigned particles represent background labeling and labeling in axonal fibers (Kulik et al., 2002). The immunogold particle density in $1^{-/-}$ mice, which completely lack $GABA_{B1}$ protein (Schuler et al., 2001), was 7% of that seen in wild-type mice. The presynaptic percentage of particles allocated to the plasma membrane in $1^{-/-}$ mice was 52%, thus showing that background labeling equally distributes over pre- and postsynaptic membranes. Only asymmetrical (glutamatergic) synapses were analyzed. An ultrastructural analysis of GABAergic (symmetrical) synapses in $1a^{-/-}$ and $1b^{-/-}$ mice was impossible due to infrequent $GABA_{B1}$ immunogold labeling (Kulik et al., 2002, 2003). The experimenter was aware of the genotype of the mice.

Transfection of Organotypic Slice Cultures and Two-Photon Laser Scanning Microscopy

Organotypic hippocampal slices were prepared from Wistar rats at postnatal day 5 as described (Stoppini et al., 1991). After 7 days in vitro, cultures were biolistically transfected with a Helios Gene Gun (Bio-Rad, CA) with $GABA_{B1a}$-GFP or $GABA_{B1b}$-GFP expression vectors in combination with a tdimer2 expression vector (gift from R. Tsien). Expression of $GABA_{B1a}$-GFP and $GABA_{B1b}$-GFP was under control of the neuron-specific *synapsin-1* promoter (gift from K. Svoboda) for 7–8 days. For imaging, we used a custom-built two-photon laser scanning microscope based on a BX51WI microscope (Olympus, Japan) and a

pulsed Ti:Sapphire laser (Chameleon XR, Coherent, Scotland) tuned to λ = 870 nm, controlled by an open source software package (ScanImage) written in Matlab (Pologruto et al., 2003). Fluorescence was detected in epifluorescence (LUMPlan W-IR2 60 × 0.9 NA, Olympus) and transfluorescence mode (achromatic aplanatic condenser, 1.4 NA, Olympus) using four photomultiplier tubes (R2896, Hamamatsu, Japan). We used 725DCXR dichroic mirrors and E700SP blocking filters to reflect emitted photons into a secondary beamsplitter, containing a 560DCXR dichroic, 525/50 (green) and 610/75 (red) band-pass filters (AHF Analysentechnik AG, Tübingen, Germany). The slice was placed into a perfusion chamber and superfused continuously (2 ml/min) with ACSF (119 mM NaCl, 2.5 mM KCl, 4 mM $CaCl_2$, 4 mM $MgCl_2$, 26.2 mM $NaHCO_3$, 1 mM NaH_2PO_4, 11 mM glucose, gassed with 95% O_2 and 5% CO_2 at room temperature). Stacks of images (256 × 256 pixels) from secondary dendritic branches and thin axons were obtained from transfected CA3 and CA1 pyramidal neurons (Z step: 0.5 μm). Maximum intensity projections of green and red stacks were constructed. For the ratio images, we used a hue/saturation/brightness model, where hue was determined by the green/red ratio (using a rainbow color table), and the intensity in the red channel was used to set the brightness. For quantitative analysis, we calculated the green-to-red ratio in a region of interest (dendrite or axon) after subtracting the background fluorescence. To compensate for differences in laser power and expression level, we normalized the ratio in the axon by the average dendritic ratio. Spines were identified by anatomy from tdimer2 images. $GABA_{B1a}$-GFP- and $GABA_{B1b}$-GFP-positive spines were defined as having intensity in the green channel at least three standard deviations above background.

Object Recognition Test

The test was designed according to the principles of Ennaceur and Delacour (1988), which rely upon the natural tendency of rodents to attend to a novel object more than a familiar one. Male wild-type (n = 7), $1a^{-/-}$ (n = 8), and $1b^{-/-}$ (n = 13) single-housed mice, aged 21 (± 0.7) weeks, were used. Mice were habituated overnight (17–21 hr) to a novel enclosure [22 × 37 × 15 (h)cm], with ~2 cm sawdust and standard food and water provided ad libitum until testing began. All sessions were recorded on video while the experimenter was out of the testing room. The number of SAPs for each mouse in each 3 min period was scored by a trained observer blinded to the animals' genotypes. All videos were scored twice by the same observer, and duplicate SAP scores were averaged within animal and time point. The intrascorer correlation (Pearson Product Moment correlation) was 0.91. A DI, the difference in SAP numbers at a pair of time points divided by the total number of SAPs at those time points, was calculated for each animal (Figure 8B). DIs reflect (1) short-term memory of a familiar object ([Number of SAPs at Time 0 min – Number of SAPs at Time 10 min]/[Total number of SAPs at both time points]); (2) longterm memory of a familiar object ([Number of SAPs at Time 0 min – Number of SAPs at Time 24 hr]/[Total number of SAPs at both time points]); and (3) short-term discriminative memory between a novel and a familiar object ([Number of SAPs at Time 24 hr + 10 min – Number of SAPs at Time 10 min]/[Total number of SAPs at both time points]). A DI of 1 reflects perfect discrimination, while a DI of 0 indicates complete loss of discrimination. SAP data were analyzed within a given genotype for the factor "Time" using the nonparametric Friedman repeated measures ANOVA on ranks test followed by Dunn's method for post hoc analysis. DIs were analyzed within a given time for the factor "Genotype" using one-way ANOVA followed by Fisher's LSD post hoc analysis.

Reagents

Tetrodotoxin (TTX) was from Latoxan (Valence, France). (R)-CPP [3-((R)-2-carboxypiperazin-4-yl)-1-phosphonic acid] and 7-chlorokynurenic acid (7-chloro-4-hydroxyquinoline-2-carboxylic acid) were from Tocris Cookson Ltd. (Bristol, UK).

Baclofen and CGP54626 were from Novartis Pharma AG (Basel, Switzerland). All other reagents were from Fluka/Sigma (Buchs, Switzerland).

Acknowledgments

This study was supported by the Swiss Science Foundation (3100-067100.01; B. Bettler), the Désirée and Nils Yde Foundation (B. Bettler), the Danish Medical Research Council (H.B.-O.), the Human Frontier Science Program (R.T), the Grant Agency of the Czech Republic (309/03/1158; R.T.), the Wellcome Trust (International Senior Research Fellowship; R.T.), and the National Institutes of Mental Health/National Institute of Drug Abuse (U01 MH69062; J.F.C., K.K., L.H.J.). We thank A. Lüthi, M. Larkum, and M. Rüegg for critical reading of the manuscript. Some of the authors of this manuscript work for Novartis Pharma AG, which has an interest in $GABA_B$ receptors as drug targets.

References

Barnes CA, Jung MW, McNaughton BL, Korol DL, Andreasson K, Worley PF. LTP saturation and spatial learning disruption: effects of task variables and saturation levels. J. Neurosci. 1994; 14:5793–5806. [PubMed: 7931545]

Bettler B, Kaupmann K, Mosbacher J, Gassmann M. Molecular structure and physiological functions of GABA(B) receptors. Physiol. Rev. 2004; 84:835–867. [PubMed: 15269338]

Bischoff S, Leonhard S, Reymann N, Schuler V, Shigemoto R, Kaupmann K, Bettler B. Spatial distribution of $GABA_BR1$ receptor mRNA and binding sites in the rat brain. J. Comp. Neurol. 1999; 412:1–16. [PubMed: 10440706]

Blein S, Ginham R, Uhrin D, Smith BO, Soares DC, Veltel S, McIlhinney RA, White JH, Barlow PN. Structural analysis of the complement control protein (CCP) modules of GABA(B) receptor 1a: only one of the two CCP modules is compactly folded. J. Biol. Chem. 2004; 279:48292–48306. [PubMed: 15304491]

Bonanno G, Raiteri M. Multiple $GABA_B$ receptors. Trends Pharmacol. Sci. 1993; 14:259–261. [PubMed: 8105595]

Bonanno G, Fassio A, Schmid G, Severi P, Sala R, Raiteri M. Pharmacologically distinct $GABA_B$ receptors that mediate inhibition of GABA and glutamate release in human neocortex. Br. J. Pharmacol. 1997; 120:60–64. [PubMed: 9117099]

Bowery NG, Bettler B, Froestl W, Gallagher JP, Marshall F, Raiteri M, Bonner TI, Enna SJ. International union of pharmacology. XXXIII. Mammalian γ-aminobutyric $acid_B$ receptors: Structure and function. Pharmacol. Rev. 2002; 54:247–264. [PubMed: 12037141]

Broadbent NJ, Squire LR, Clark RE. Spatial memory, recognition memory, and the hippocampus. Proc. Natl. Acad. Sci. USA. 2004; 101:14515–14520. [PubMed: 15452348]

Burrone J, Murthy VN. Synaptic gain control and homeostasis. Curr. Opin. Neurobiol. 2003; 13:560–567. [PubMed: 14630218]

Couve A, Thomas P, Calver AR, Hirst WD, Pangalos MN, Walsh FS, Smart TG, Moss SJ. Cyclic AMP-dependent protein kinase phosphorylation facilitates $GABA_B$ receptor-effector coupling. Nat. Neurosci. 2002; 5:415–424. [PubMed: 11976702]

Cryan JF, Kaupmann K. Don't worry 'B' happy!: a role for GABA(B) receptors in anxiety and depression. Trends Pharmacol. Sci. 2005; 26:36–43. [PubMed: 15629203]

Cunningham MD, Enna SJ. Evidence for pharmacologically distinct $GABA_B$ receptors associated with cAMP production in rat brain. Brain Res. 1996; 720:220–224. [PubMed: 8782915]

Davies CH, Collingridge GL. Regulation of EPSPs by the synaptic activation of $GABA_B$ autoreceptors in rat hippocampus. J. Physiol. 1996; 496:451–470. [PubMed: 8910229]

Davies CH, Starkey SJ, Pozza MF, Collingridge GL. GABA autoreceptors regulate the induction of LTP. Nature. 1991; 349:609–611. [PubMed: 1847993]

Deisz RA, Billard JM, Zieglgansberger W. Presynaptic and postsynaptic $GABA_B$ receptors of neocortical neurons of the rat in vitro: differences in pharmacology and ionic mechanisms. Synapse. 1997; 25:62–72. [PubMed: 8987149]

Europe PMC Funders Author Manuscripts

Dinkel A, Aicher WK, Warnatz K, Burki K, Eibel H, Ledermann B. Efficient generation of transgenic BALB/c mice using BALB/c embryonic stem cells. J. Immunol. Methods. 1999; 223:255–260. [PubMed: 10089104]

Durand GM, Kovalchuk Y, Konnerth A. Long-term potentiation and functional synapse induction in developing hippocampus. Nature. 1996; 381:71–75. [PubMed: 8609991]

Ennaceur A, Delacour J. A new one-trial test for neuro-biological studies of memory in rats. 1: Behavioral data. Behav. Brain Res. 1988; 31:47–59. [PubMed: 3228475]

Fritschy JM, Sidler C, Parpan F, Gassmann M, Kaupmann K, Bettler B, Benke D. Independent maturation of the GABA(B) receptor subunits GABA(B1) and GABA(B2) during postnatal development in rodent brain. J. Comp. Neurol. 2004; 477:235–252. [PubMed: 15305362]

Gasparini S, Saviane C, Voronin LL, Cherubini E. Silent synapses in the developing hippocampus: lack of functional AMPA receptors or low probability of glutamate release? Proc. Natl. Acad. Sci. USA. 2000; 97:9741–9746. [PubMed: 10931951]

Gassmann M, Shaban H, Vigot R, Sansig G, Haller C, Barbieri S, Humeau Y, Schuler V, Muller M, Kinzel B, et al. Redistribution of GABAB(1) protein and atypical GABAB responses in GABAB(2)-deficient mice. J. Neurosci. 2004; 24:6086–6097. [PubMed: 15240800]

Gemignani A, Paudice P, Bonanno G, Raiteri M. Pharmacological discrimination between gamma-aminobutyric acid type B receptors regulating cholecystokinin and somatostatin release from rat neocortex synaptosomes. Mol. Pharmacol. 1994; 46:558–562. [PubMed: 7935338]

Grace CR, Perrin MH, DiGruccio MR, Miller CL, Rivier JE, Vale WW, Riek R. NMR structure and peptide hormone binding site of the first extracellular domain of a type B1 G protein-coupled receptor. Proc. Natl. Acad. Sci. USA. 2004; 101:12836–12841. [PubMed: 15326300]

Horton AC, Ehlers MD. Neuronal polarity and trafficking. Neuron. 2003; 40:277–295. [PubMed: 14556709]

Isaac JT, Nicoll RA, Malenka RC. Evidence for silent synapses: implications for the expression of LTP. Neuron. 1995; 15:427–434. [PubMed: 7646894]

Kaupmann K, Huggel K, Heid J, Flor PJ, Bischoff S, Mickel SJ, McMaster G, Angst C, Bittiger H, Froestl W, Bettler B. Expression cloning of $GABA_B$ receptors uncovers similarity to metabotropic glutamate receptors. Nature. 1997; 386:239–246. [PubMed: 9069281]

Kaupmann K, Malitschek B, Schuler V, Heid J, Froestl W, Beck P, Mosbacher J, Bischoff S, Kulik A, Shigemoto R, et al. $GABA_B$-receptor subtypes assemble into functional heteromeric complexes. Nature. 1998; 396:683–687. [PubMed: 9872317]

Kulik A, Nakadate K, Nyiri G, Notomi T, Malitschek B, Bettler B, Shigemoto R. Distinct localization of $GABA_B$ receptors relative to synaptic sites in the rat cerebellum and ventrobasal thalamus. Eur. J. Neurosci. 2002; 15:291–307. [PubMed: 11849296]

Kulik A, Vida I, Lujan R, Haas CA, Lopez-Bendito G, Shigemoto R, Frotscher M. Subcellular localization of metabotropic $GABA_B$ receptor subunits $GABA_{B(1a/b)}$ and $GABA_{B(2)}$ in the rat hippocampus. J. Neurosci. 2003; 23:11026–11035. [PubMed: 14657159]

Kulik A, Vida I, Fukuzawa Y, Guetg N, Kasugai Y, Marker CL, Rigato F, Bettler B, Wickman K, Frotscher M, Shigemoto R. Compartment-dependent colocalization of Kir3.2-containing K+ channels and GABAB receptors in hippocampal pyramidal cells. J. Neurosci. 2006; 26:4289–4297. [PubMed: 16624949]

Kullmann DM. Amplitude fluctuations of dual-component EPSCs in hippocampal pyramidal cells: implications for long-term potentiation. Neuron. 1994; 12:1111–1120. [PubMed: 7910467]

Lehtinen MJ, Meri S, Jokiranta TS. Interdomain contact regions and angles between adjacent short consensus repeat domains. J. Mol. Biol. 2004; 344:1385–1396. [PubMed: 15561150]

Lei S, McBain CJ. GABA B receptor modulation of excitatory and inhibitory synaptic transmission onto rat CA3 hippocampal interneurons. J. Physiol. 2003; 546:439–453. [PubMed: 12527730]

Liao D, Hessler NA, Malinow R. Activation of postsynaptically silent synapses during pairing-induced LTP in CA1 region of hippocampal slice. Nature. 1995; 375:400–404. [PubMed: 7760933]

Liao D, Zhang X, O'Brien R, Ehlers MD, Huganir RL. Regulation of morphological postsynaptic silent synapses in developing hippocampal neurons. Nat. Neurosci. 1999; 2:37–43. [PubMed: 10195178]

Lüscher C, Jan LY, Stoffel M, Malenka RC, Nicoll RA. G protein-coupled inwardly rectifying K^+ channels (GIRKs) mediate postsynaptic but not presynaptic transmitter actions in hippocampal neurons. Neuron. 1997; 19:687–695. [PubMed: 9331358]

Luthi A, Schwyzer L, Mateos JM, Gahwiler BH, McKinney RA. NMDA receptor activation limits the number of synaptic connections during hippocampal development. Nat. Neurosci. 2001; 4:1102–1107. [PubMed: 11687815]

Malinow R, Malenka RC. AMPA receptor trafficking and synaptic plasticity. Annu. Rev. Neurosci. 2002; 25:103–126. [PubMed: 12052905]

Malitschek B, Rüegg D, Heid J, Kaupmann K, Bittiger H, Fröstl W, Bettler B, Kuhn R. Developmental changes in agonist affinity at $GABA_{B(1)}$ receptor variants in rat brain. Mol. Cell. Neurosci. 1998; 12:56–64. [PubMed: 9770340]

Marshall FH, Jones KA, Kaupmann K, Bettler B. $GABA_B$ receptors—the first 7TM heterodimers. Trends Pharmacol. Sci. 1999; 20:396–399. [PubMed: 10498952]

Martin SC, Russek SJ, Farb DH. Human $GABA_{B(R)}$ genomic structure: evidence for splice variants in $GABA_{B(R1)}$ but not $GABA_{B(R2)}$. Gene. 2001; 278:63–79. [PubMed: 11707323]

McLatchie LM, Fraser NJ, Main MJ, Wise A, Brown J, Thompson N, Solari R, Lee MG, Foord SM. RAMPs regulate the transport and ligand specificity of the calcitonin-receptor-like receptor. Nature. 1998; 393:333–339. [PubMed: 9620797]

Mintz IM, Bean BP. $GABA_B$ receptor inhibition of P-type Ca^{2+} channels in central neurons. Neuron. 1993; 10:889–898. [PubMed: 8388225]

Mohler H, Fritschy JM. GABAB receptors make it to the top—as dimers. Trends Pharmacol. Sci. 1999; 20:87–89. [PubMed: 10203861]

Morrisett RA, Mott DD, Lewis DV, Swartzwelder HS, Wilson WA. $GABA_B$-receptor-mediated inhibition of the N-methyl-D-aspartate component of synaptic transmission in the rat hippocampus. J. Neurosci. 1991; 11:203–209. [PubMed: 1846009]

Palmer MJ, Isaac JT, Collingridge GL. Multiple, developmentally regulated expression mechanisms of long-term potentiation at CA1 synapses. J. Neurosci. 2004; 24:4903–4911. [PubMed: 15163681]

Pérez-Garci E, Gassmann M, Bettler B, Larkum ME. The $GABA_{B1b}$ isoform mediates long-lasting inhibition of dendritic Ca^{2+} spikes in layer 5 somatosensory pyramidal neurons. Neuron. 2006; 50(this issue):603–616. [PubMed: 16701210]

Pineda VV, Athos JI, Wang H, Celver J, Ippolito D, Boulay G, Birnbaumer L, Storm DR. Removal of G(iα1)constraints on adenylyl cyclase in the hippocampus enhances LTP and impairs memory formation. Neuron. 2004; 41:153–163. [PubMed: 14715142]

Pologruto TA, Sabatini BL, Svoboda K. ScanImage: flexible software for operating laser scanning microscopes. Biomed. Eng. Online. 2003; 2:13. [PubMed: 12801419]

Poncer JC, McKinney RA, Gahwiler BH, Thompson SM. Either N- or P-type calcium channels mediate GABA release at distinct hippocampal inhibitory synapses. Neuron. 1997; 18:463–472. [PubMed: 9115739]

Pozza MF, Manuel NA, Steinmann M, Froestl W, Davies CH. Comparison of antagonist potencies at pre- and postsynaptic $GABA_B$ receptors at inhibitory synapses in the CA1 region of the rat hippocampus. Br. J. Pharmacol. 1999; 127:211–219. [PubMed: 10369475]

Prosser HM, Gill CH, Hirst WD, Grau E, Robbins M, Calver A, Soffin EM, Farmer CE, Lanneau C, Gray J, et al. Epileptogenesis and enhanced prepulse inhibition in $GABA_{B(1)}$-deficient mice. Mol. Cell. Neurosci. 2001; 17:1059–1070. [PubMed: 11414794]

Sakaba T, Neher E. Direct modulation of synaptic vesicle priming by $GABA_B$ receptor activation at a glutamatergic synapse. Nature. 2003; 424:775–778. [PubMed: 12917685]

Sampo B, Kaech S, Kunz S, Banker G. Two distinct mechanisms target membrane proteins to the axonal surface. Neuron. 2003; 37:611–624. [PubMed: 12597859]

Scanziani M. GABA spillover activates postsynaptic GABA(B) receptors to control rhythmic hippocampal activity. Neuron. 2000; 25:673–681. [PubMed: 10774734]

Schuler V, Lüscher C, Blanchet C, Klix N, Sansig G, Klebs K, Schmutz M, Heid J, Gentry C, Urban L, et al. Epilepsy, hyperalgesia, impaired memory, and loss of pre- and postsynaptic $GABA_B$ responses in mice lacking $GABA_{B(1)}$. Neuron. 2001; 31:47–58. [PubMed: 11498050]

Scimemi A, Fine A, Kullmann DM, Rusakov DA. NR2B-containing receptors mediate cross talk among hippocampal synapses. J. Neurosci. 2004; 24:4767–4777. [PubMed: 15152037]

Steiger JL, Bandyopadhyay S, Farb DH, Russek SJ. cAMP response element-binding protein, activating transcription factor-4, and upstream stimulatory factor differentially control hippocampal GABABR1a and GABABR1b subunit gene expression through alternative promoters. J. Neurosci. 2004; 24:6115–6126. [PubMed: 15240803]

Stoppini L, Buchs PA, Muller D. A simple method for organotypic cultures of nervous tissue. J. Neurosci. Methods. 1991; 37:173–182. [PubMed: 1715499]

West AE, Griffith EC, Greenberg ME. Regulation of transcription factors by neuronal activity. Nat. Rev. Neurosci. 2002; 3:921–931. [PubMed: 12461549]

Xiao MY, Wasling P, Hanse E, Gustafsson B. Creation of AMPA-silent synapses in the neonatal hippocampus. Nat. Neurosci. 2004; 7:236–243. [PubMed: 14966524]

Yamada K, Yu B, Gallagher JP. Different subtypes of $GABA_B$ receptors are present at pre- and postsynaptic sites within the rat dorsolateral septal nucleus. J. Neurophysiol. 1999; 81:2875–2883. [PubMed: 10368404]

Europe PMC Funders Author Manuscripts

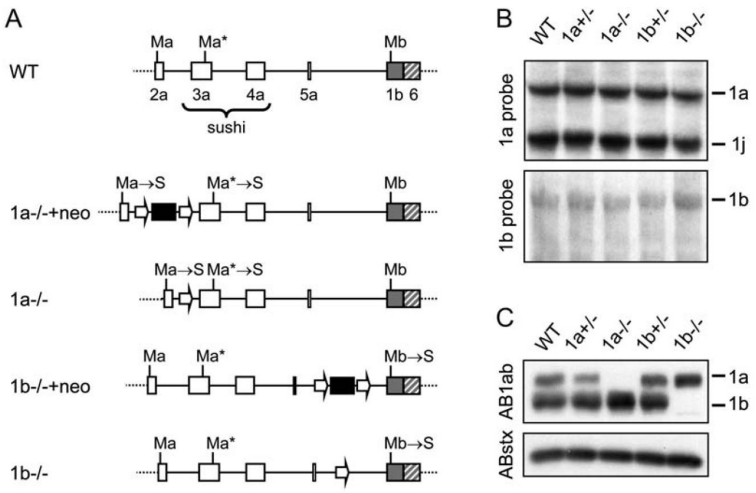

Figure 1. Generation of $1a^{-/-}$ and $1b^{-/-}$ Mice

(A) 5′ region of wild-type (WT) (Martin et al., 2001) and mutated *GABA*$_{B1}$ alleles. Exons encoding the N terminus of $GABA_{B1a}$ are represented by white boxes and specify the signal peptide (exon 2a), a pair of sushi repeats of 75 amino acids each (exons 3a, 4a), and a linker of six amino acids (exon 5a). The exon specifying the N terminus of $GABA_{B1b}$ is represented by a gray box. All exons downstream of exon 1b are shared between the two isoforms (only exon 6 is shown; hatched box). Start codons for *GABA*$_{B1a}$ (Ma) and *GABA*$_{B1b}$ (Mb) transcripts were converted into stop codons (S) using a knockin approach. A putative alternative start site (Ma*) in *GABA*$_{B1a}$ transcripts was mutated in addition. The floxed neomycin cassette (black bar) for selection of transfected embryonic stem cells was introduced in the introns between exons 2a/3a ($1a^{-/-}$neo) or exons 5a/1b ($1b^{-/-}$neo). A loxP site (arrow) is left behind after Cre-mediated excision of the neomycin cassette ($1a^{-/-}$, $1b^{-/-}$).

(B) Northern blot analysis of *GABA*$_{B1a}$ and *GABA*$_{B1b}$ mRNA expression in the brain of WT, heterozygous ($^{+/-}$), and homozygous ($^{-/-}$) knockout mice. The 1a hybridization probe (1a probe) corresponds to nucleotides 1–405 of the *GABA*$_{B1a}$ cDNA (Kaupmann et al., 1997) and detects *GABA*$_{B1a}$ as well as a truncated *GABA*$_{B1j}$ transcript (M.G., unpublished data) of ~1.6 kb (upper panel). The 1b probe corresponds to nucleotides 16–259 of the *GABA*$_{B1b}$ cDNA (Kaupmann et al., 1997) and detects 1b transcripts (lower panel).

(C) Immunoblot analysis of total brain lysates using antibodies recognizing the common C terminus of $GABA_{B1a}$ and $GABA_{B1b}$ (AB1ab) (Gassmann et al., 2004). Anti-syntaxin (ABstx) antibodies control for sample loading.

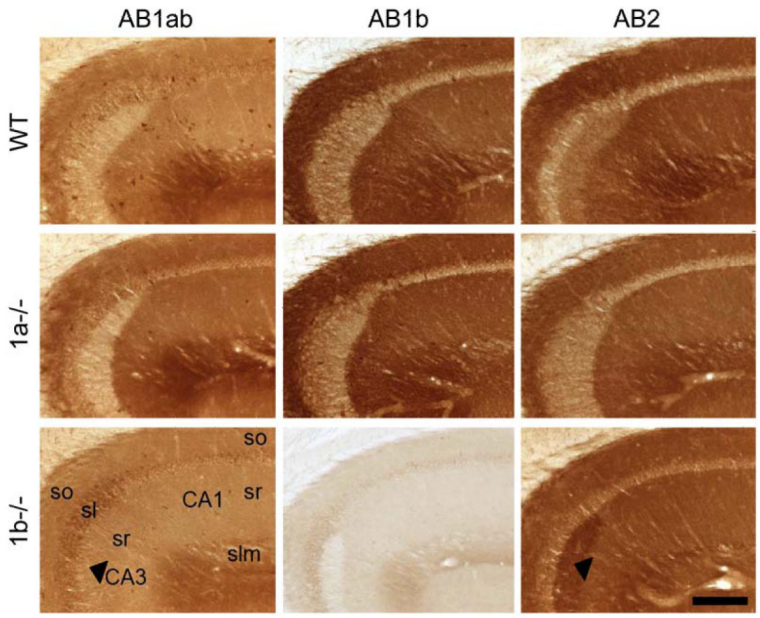

Figure 2. Distribution of $GABA_{B1a}$ and $GABA_{B1b}$ Protein in the Hippocampus of $1a^{-/-}$ and $1b^{-/-}$ Mice

Immunohistochemistry in the CA1/CA3 region using antibodies specific for $GABA_{B1}$ (AB1ab, recognizing an epitope shared by $GABA_{B1a}$ and $GABA_{B1b}$), $GABA_{B1b}$ (AB1b), and $GABA_{B2}$ (AB2). No $GABA_{B1a}$-specific antibody suitable for immunohistochemistry is available. The expression pattern of $GABA_{B1a}$ protein is revealed in $1b^{-/-}$ mice stained with AB1ab. No specific immunostaining is observed with AB1b in $1b^{-/-}$ mice, demonstrating the specificity of this antibody for $GABA_{B1b}$ protein. No specific immunostaining was obtained in control experiments with AB1ab/AB1b and AB2 antibodies in mice devoid of $GABA_{B1}$ and $GABA_{B2}$ subunits, respectively (Fritschy et al., 2004). Abbreviations: so, stratum oriens; sl, stratum lucidum; sr, stratum radiatum; slm, stratum lacunosum-moleculare. Scale bar, 200 μm. The WT mouse was a littermate of the $1a^{-/-}$ mouse.

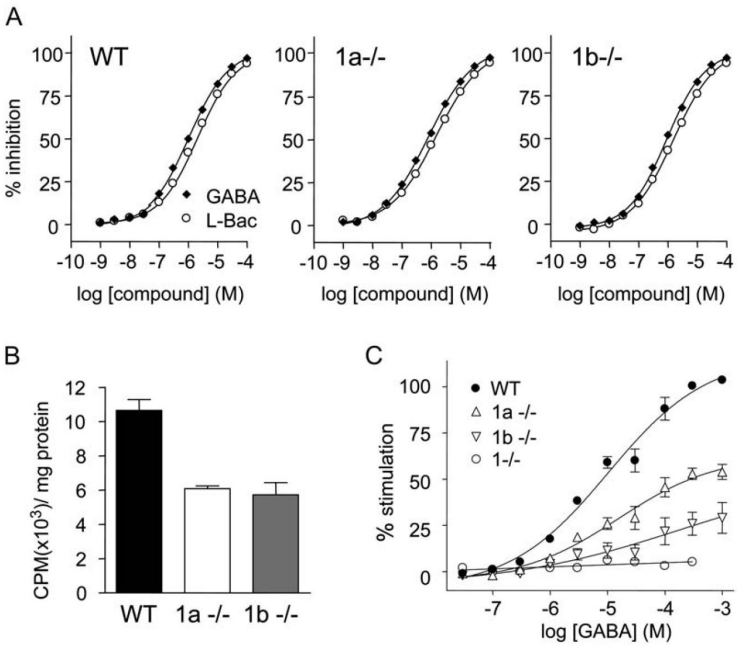

Figure 3. Pharmacological and Biochemical Analysis of Brain Membranes from Wild-Type, *1a*$^{-/-}$, and *1b*$^{-/-}$ Mice

(A) Inhibition of [^{125}I]CGP64213 $GABA_B$ antagonist binding to cortical membranes by the agonists GABA and L-baclofen (L-Bac). The curves were fitted using nonlinear regression (Graph Pad PRISM program, Graph Pad software Inc., San Diego). Error bars (±SEM) are smaller than the symbols.

(B) Binding of [^{3}H]baclofen to cortical membranes of *1a*$^{-/-}$ and *1b*$^{-/-}$ mice was 57% ± 2% and 50% ± 7%, respectively, of the binding to WT membranes (±SEM of two independent experiments performed in triplicate).

(C) GABA-stimulated GTPγ[^{35}S] binding in cortical membranes. Data points are mean (±SEM) values calculated from five (WT) and four (*1a*$^{-/-}$, *1b*$^{-/-}$, 1$^{-/-}$) mice.

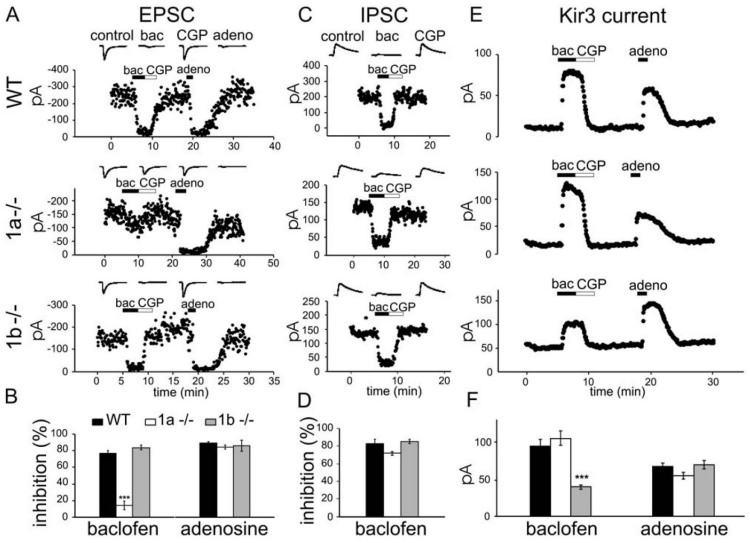

Figure 4. $GABA_B$ Responses in Wild-Type, $1a^{-/-}$, and $1b^{-/-}$ CA1 Pyramidal Neurons

(A and B) Peak amplitudes and representative traces (A) and summary histogram (B) of monosynaptic EPSC inhibition by baclofen and adenosine. Baclofen (50 μM) depresses the amplitude of EPSCs in WT (76.5% ± 3.1% inhibition; n = 8) and $1b^{-/-}$ (83.4% ± 2.9% inhibition; n = 5) but not in $1a^{-/-}$ (15.9% ± 5.3% inhibition; n = 13; $p < 0.001$, ANOVA/Scheffe post hoc test) mice. Adenosine (100 μM) depresses EPSCs in all genotypes (WT: 89.1% ± 1.6% inhibition, n = 6; $1a^{-/-}$: 85.3% ± 1.8% inhibition, n = 13; $1b^{-/-}$: 85.6% ± 6.6% inhibition, n = 4).

(C and D) Peak amplitudes and representative traces (C) and summary histogram (D) of IPSC inhibition by baclofen. Baclofen significantly depresses the IPSC amplitude in all genotypes (WT: 82.7% ± 4.8% inhibition, n = 12; $1a^{-/-}$: 71.8% ± 2.3% inhibition, n = 9; $1b^{-/-}$ mice: 85.7% ± 2.4% inhibition, n = 7).

(E and F) Representative changes in the holding current of CA1 neurons following application of baclofen and adenosine (E) and summary histogram of the amplitude of baclofen- and adenosine-induced K^+ currents (F). The amplitude of the outward K^+ current induced by baclofen application is similar in $1a^{-/-}$ (99.3 ± 8.8 pA; n = 14) and WT (89.8 ± 7.7 pA; n = 16) neurons. In $1b^{-/-}$ cells, the amplitude of the baclofen-induced current is strongly reduced (37.4 ± 2.7 pA; n = 10; $p < 0.001$, ANOVA/Scheffe post hoc test). Control adenosine-induced K^+ currents are similar in all genotypes. (Vclamp: −50 mV, TTX 1 μM, ***$p < 0.001$, ANOVA/Scheffe post hoc test). All baclofen-induced responses (inhibition of PSCs and activation of K^+ currents) were fully blocked by the $GABA_B$ antagonist CGP54626 (1 μM). Values are expressed as mean ± SEM.

Europe PMC Funders Author Manuscripts

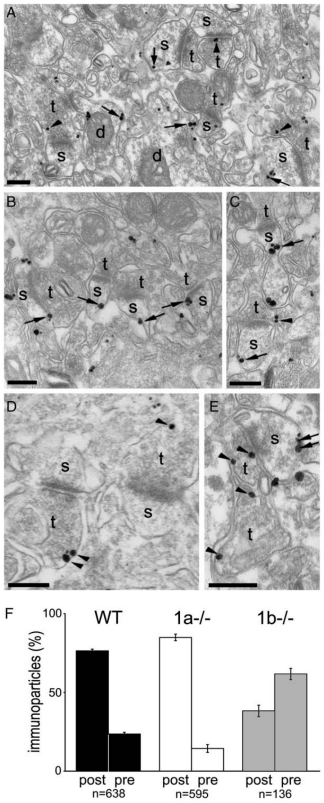

Figure 5. Preembedding Electron Micrographs Showing $GABA_{B1}$ Immunogold Labeling at Asymmetrical, i.e. Glutamatergic, Synapses in CA1 Stratum Radiatum

(A) Pre- and postsynaptic immunogold labeling in WT mice.

(B and C) Predominant postsynaptic (B) and rare presynaptic (C) labeling (arrowhead) in $1a^{-/-}$ mice.

(D and E) Predominant presynaptic (D) and less frequent postsynaptic (E) labeling in $1b^{-/-}$ mice.

(F) Percentage of pre- and postsynaptic immunogold particles in WT, $1a^{-/-}$, and $1b^{-/-}$ mice (presynaptic: WT, 24% ± 1%; $1a^{-/-}$, 14% ± 3%; $1b^{-/-}$, 62% ± 4%; n = 3 for each genotype; mean ± SEM). Immunogold labeling was less frequent in $1b^{-/-}$ compared to $1a^{-/-}$ mice, which is reflected in the number of immunogold particles that were analyzed. Arrow: examples of immunogold particles in spines and dendritic shafts; arrowhead: examples of immunogold particles in presynaptic terminals. t, terminal; s, spine; d, dendrite; scale bars, 200 nm.

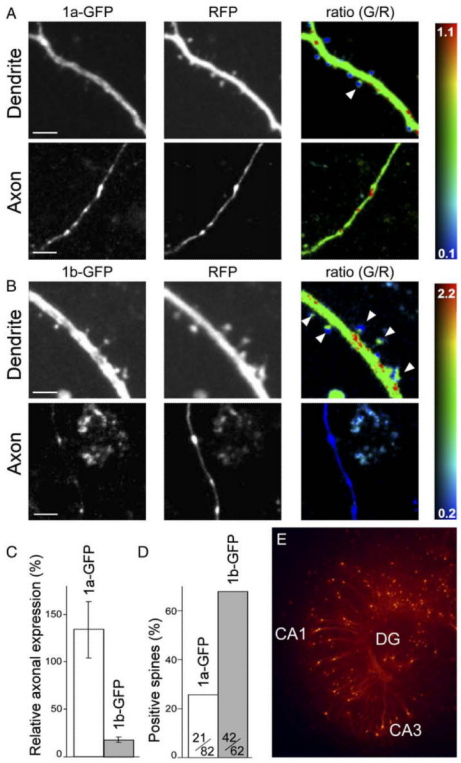

Figure 6. Expression of GFP-Tagged$GABA_{B1a}$ and $GABA_{B1b}$ Subunits in Organotypic Slice Culture

Maximum intensity projections of dendrites and axons in the CA1 region of the hippocampus expressing $GABA_{B1a}$-GFP (A) or $GABA_{B1b}$-GFP (B) in combination with the freely diffusible tdimer2 RFP are shown. The ratio of green-to-red fluorescence (G/R) is coded in rainbow colors. Scale bar, 5 μm. (C) Predominantly $GABA_{B1a}$-GFP protein is expressed in axons. The axonal expression level of $GABA_{B1a}$ and $GABA_{B1b}$ was normalized to the dendritic expression level ($GABA_{B1a}$: 133.84% ± 29.53%, n = 9; $GABA_{B1b}$: 18.01% ± 2.80%, n = 5; mean ± SEM). (D) $GABA_{B1b}$-GFP was expressed in the majority of dendritic spines, while $GABA_{B1a}$-GFP was excluded from most spines (spines positive for $GABA_{B1a}$-GFP: 21 of 82; spines positive for $GABA_{B1b}$-GFP: 42 of 62). Examples of positive spines are indicated by white arrowheads in the G/R ratio images in (A) and (B). (E) Example of an organotypic hippocampal slice culture 7 days after cotransfection of $GABA_{B1b}$-GFP and tdimer2 expression vectors.

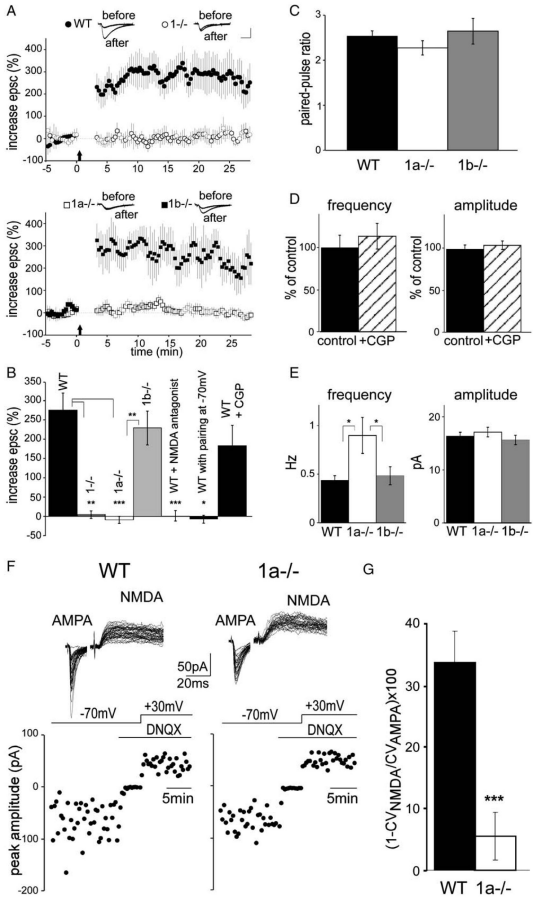

Figure 7. Lack of LTP and Reduction in the Proportion of Silent Synapses in *1a*$^{-/-}$ Mice

(A) The pairing protocol fails to induce LTP in 1$^{-/-}$ and *1a*$^{-/-}$ mice but induces a clear potentiation of the EPSC amplitude in WT and *1b*$^{-/-}$ mice. Averages of the maximal EPSC amplitudes (±SEM) are shown. Pairing induction is indicated with an arrow. (Insets) Mean of 10 to 15 successive EPSCs recorded before and after pairing. Scale, 20 ms, 50 pA. (B) Summary histogram of LTP experiments. The percent increase in EPSC amplitude after pairing is shown. Values for EPSC potentiation were assessed 25 min after induction. No LTP is induced in WT mice in the presence of NMDA antagonists (5 μM R-CPP + 10 μM 7-Cl-kynurenate; WT + NMDA antagonist; $p < 0.001$ compared to WT, Student's t test) and in the absence of paradigm-associated depolarization (WT with pairing at −70 mV; $p < 0.05$ compared to WT, Student's t test). LTP is not significantly impaired in the presence of 1 μM CGP54626 (WT +CGP). The ANOVA/Scheffe post hoc test was used for the comparison of genotypes. For clarity, only the statistical significance between the genotypes linked by the brackets are shown (*$p < 0.05$; **$p < 0.01$; ***$p < 0.001$). (C) The pairedpulse ratio of EPSCs at CA3-to-CA1 synapses in WT (2.54 ± 0.11; n = 15), *1a*$^{-/-}$ (2.27 ± 0.16; n = 15) and *1b*$^{-/-}$ (2.64 ± 0.28; n = 8) mice was similar. (D) The $GABA_B$ antagonist CGP54626 (1 μM) did not alter mEPSC frequency (increase of 13.6% ± 15.3% versus control; n = 11) or amplitude (increase of 4.3% ± 5.1%; n = 11) in WT mice. (E) The frequency of mEPSCs was increased in *1a*$^{-/-}$ mice (WT: 0.44 ± 0.05 Hz, n = 11; *1a*$^{-/-}$: 0.90 ± 0.14 Hz, n = 15; *1b*$^{-/-}$: 0.49 ± 0.09 Hz, n = 8; $p < 0.05$, Student's t test). In contrast, the mEPSC amplitude did not differ between WT (16.39 ± 0.79 pA; n = 11), *1a*$^{-/-}$ (17.12 ± 0.78 pA; n = 18), and *1b*$^{-/-}$ (15.68 ± 0.88 pA; n = 8) mice. (F) Raw traces of AMPA and NMDA receptor-mediated EPSCs components (top). The protocol used to determine the CV_{AMPA} and

Europe PMC Funders Author Manuscripts

CV_{NMDA} is outlined. At −70 mV, NMDA receptors are blocked by Mg^{2+} ions, and the EPSCs are primarily mediated by AMPA receptors. NMDA receptor-mediated EPSCs were recorded in the same cell at +30 mV in the presence of 10 μM DNQX, a non-NMDA receptor antagonist. (G) The variability of the AMPA compared to the NMDA EPSC component (calculated as $[1 – (CV_{NMDA}/CV_{AMPA})] \times 100$) is significantly smaller in *1a*$^{-/-}$ than in WT mice (WT: 34.0 ± 5.0, n = 12; *1a*$^{-/-}$: 5.6 ± 3.9, n = 10; $p < 0.01$, Student's t test), suggestive of a decreased proportion of silent synapses. WT mice were littermates of *1a*$^{-/-}$ mice. Data are represented as mean ± SEM.

Europe PMC Funders Author Manuscripts

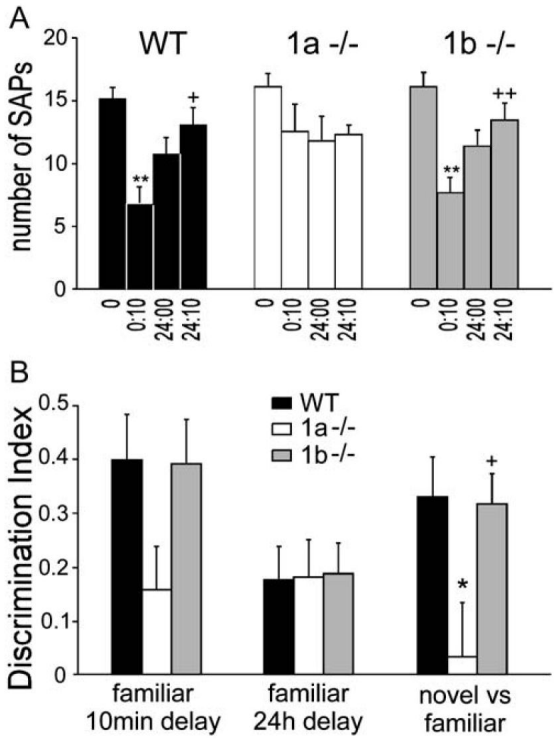

Figure 8. Impaired Object Recognition in *1a*$^{-/-}$ Mice

(A) Data represent the number of SAPs (mean ± SEM) to a PVC disc presented at time 0 min (0), 10 min (0:10), and 24 hr (24:00), and to a novel PVC cone at 24 hr + 10 min (24:10). **p < 0.01 versus 0 min; +p < 0.05 versus 10 min; ++p < 0.01 versus 10 min. *1a*$^{-/-}$ mice do not discriminate between familiar and novel objects (χ^2 = 5.824, 3 df, p = 0.121), in contrast to WT (χ^2 = 13.80, 3 df, p = 0.003) and *1b*$^{-/-}$ mice (χ^2 = 23.016, 3 df, p < 0.001). This deficit of *1a*$^{-/-}$ mice was also evident in a separate cohort of mice (data not shown). (B) Discrimination indices (DIs; mean ± SEM) in the object recognition test for WT, *1a*$^{-/-}$, and *1b*$^{-/-}$ mice. Time points for calculating DIs were chosen to reflect the following: short-term memory of a familiar object (familiar 10 min delay), long-term memory of a familiar object (familiar 24 hr delay), and short-term discriminative memory between a novel and familiar object (novel versus familiar). The mean DI for discrimination of a familiar object after 10 min delay appeared to be lower in *1a*$^{-/-}$ mice but failed to meet statistical significance [DI: F(2, 26) = 2.006; p = 0.149]. However, the decrease in the mean DI for discrimination of a novel versus a familiar object is significantly lower in *1a*$^{-/-}$ mice than in *1b*$^{-/-}$ or WT mice [F(2, 26) = 4.404; p = 0.023]. After a delay of 24 hr, the three genotypes similarly demonstrated a lack of familiarity with the previously presented disc [DI: F(2, 26) = 0.001; p = 0.999]. *p = 0.05 versus WT; +p < 0.05 versus *1a*$^{-/-}$.

Europe PMC Funders Author Manuscripts